Copy 262
RM L53I29a

NACA

RESEARCH MEMORANDUM

STATIC LATERAL STABILITY CHARACTERISTICS OF A 1/16-SCALE MODEL OF THE DOUGLAS D-558-II RESEARCH AIRPLANE AT MACH NUMBERS OF 1.61 AND 2.01

By Frederick C. Grant and Ross B. Robinson

Langley Aeronautical Laboratory
Langley Field, Va.

NATIONAL ADVISORY COMMITTEE FOR AERONAUTICS

WASHINGTON

November 4, 1953

NATIONAL ADVISORY COMMITTEE FOR AERONAUTICS

RESEARCH MEMORANDUM

STATIC LATERAL STABILITY CHARACTERISTICS OF A 1/16-SCALE MODEL OF THE DOUGLAS D-558-II RESEARCH AIRPLANE AT MACH NUMBERS OF 1.61 AND 2.01

By Frederick C. Grant and Ross B. Robinson

SUMMARY

Results of tests of a 1/16-scale model of the Douglas D-558-II research airplane which were made in the Langley 4- by 4-foot supersonic pressure tunnel at Mach numbers of 1.61 and 2.01 have indicated that the complete model has positive directional stability and positive effective dihedral at both Mach numbers with no significant change in the directional stability or effective dihedral with Mach number. The apparent differences in trend between flight and tunnel test results are believed to be due to the difficulty experienced in measuring the directional-stability derivative C_{n_β} in flight during combined rolling and yawing motions.

As predicted by theory, the rudder effectiveness was less at the higher Mach number.

Addition of the wing to the body—vertical-tail configuration reduced the lateral force and yawing moment of the tail but increased the incremental rolling moment due to the tail.

INTRODUCTION

Tests have been made in the Langley 4- by 4-foot supersonic pressure tunnel to determine the aerodynamic characteristics of a 1/16-scale model of the Douglas D-558-II research airplane. These tunnel tests supplement the flight tests of the D-558-II which are being conducted at the NACA High-Speed Flight Research Station. The flight tests have indicated that the directional stability of the D-558-II is low at supersonic speeds and decreases rapidly as the Mach number increases. The purpose of the wind-tunnel tests was to determine the static lateral stability characteristics of the complete model at Mach numbers of 1.61 and 2.01 and the contributions to the static-lateral-stability derivatives of the components of the model.

Results of low subsonic Mach number tunnel tests of a 0.25-scale model are given in reference 1, while the longitudinal stability and control characteristics of the present model at high subsonic and low supersonic speeds are given in reference 2. The static longitudinal stability and control characteristics at Mach numbers of 1.61 and 2.01 are presented in reference 3. Calculations of the dynamic lateral stability characteristics of the full-scale airplane are presented in references 4 and 5 up to high subsonic and supersonic Mach numbers, respectively. Flight-test results showing the lateral stability and control characteristics of the airplane through the Mach number range of 0.27 to 1.87 are given in references 6 to 11.

The present paper gives the aerodynamic characteristics in sideslip at angles of attack of 0° and 4° for the complete 1/16-scale model and for combinations of its components at Mach numbers of 1.61 and 2.01. At these Mach numbers, the Reynolds numbers (based on the mean aerodynamic chord) were 1.90×10^6 and 1.52×10^6, respectively. Analysis of the results obtained was limited to comparisons of the experimental results with calculations for the complete airplane of reference 5 and estimates of the body-alone characteristics using the method of reference 12.

COEFFICIENTS AND SYMBOLS

The results of the tests are presented in terms of standard NACA coefficients of forces and moments which are referred to the stability-axes system (fig. 1). The coefficients and symbols used are defined as follows:

C_L lift coefficient, $-Z/qS$

C_X longitudinal-force coefficient, X/qS

C_Y lateral-force coefficient, Y/qS

C_l rolling-moment coefficient, L/qSb

C_m pitching-moment coefficient, $M'/qS\bar{c}$

C_n yawing-moment coefficient, N/qSb

X	force along X-axis
Y	force along Y-axis
Z	force along Z-axis
L	moment about X-axis
M'	moment about Y-axis
N	moment about Z-axis
q	free-stream dynamic pressure
S	total wing area including body intercept
b	wing span
$\bar{c}$	wing mean aerodynamic chord, $\int_0^{b/2} c^2 dy \Big/ \int_0^{b/2} c\, dy$
M	Mach number
p	angular velocity about X-axis
ϕ	roll angle, $\int p\, dt$
α	angle of attack of body center line, deg
β	angle of sideslip, deg
δ_r	rudder deflection, deg
i_t	stabilizer deflection, deg
δ_e	elevator deflection, deg

$$C_{Y_\beta} = \frac{\partial C_Y}{\partial \beta}$$

$$C_{n_\beta} = \frac{\partial C_n}{\partial \beta}$$

$C_{l_\beta} = \frac{\partial C_l}{\partial \beta}$

$\left(\Delta C_Y\right)_t$ increment of lateral-force coefficient due to addition of vertical tail

$\left(\Delta C_n\right)_t$ increment of yawing-moment coefficient due to addition of vertical tail

$\left(\Delta C_l\right)_t$ increment of rolling-moment coefficient due to addition of vertical tail

MODEL AND APPARATUS

A three-view drawing of the model is shown in figure 2 and the details of the wing fences are shown in figure 3. The vertical tail of the model is the same as that originally used on the airplane (refs. 1 to 4). However, a slightly extended tail and slightly smaller rudder are now employed on the airplane (refs. 5 to 11). In addition, the after-portion of the fuselage of the model was enlarged to accommodate the balance. These alterations are shown in figure 4. A photograph of the model in the tunnel is shown in figure 5. The geometric characteristics of the model are presented in table I. Coordinates for the body are given in table II and for the wing fences in table III.

The model had a wing without ailerons, with 35° of sweep of the 0.30-chord line of the unswept panel, aspect ratio 3.57, taper ratio 0.565, and NACA 63-010 airfoil sections normal to the 0.30-chord line. The wing was at 3° incidence to the fuselage center line and had 3° of negative dihedral.

The horizontal tail, the elevators, and the rudder were movable, and the deflections of these surfaces were set manually. The wing, vertical tail, and horizontal tail of the model were removable so that tests of combinations of components could be made. Force and moment measurements were made with a six-component internal strain-gage balance. No hinge-moment data were taken on any of the control surfaces.

The model was mounted on a 4° bent sting. By using the bent sting, it was possible to test through the angle-of-attack range at sideslip angles of 0° and 4° and through the sideslip angle range at angles of attack of 0° and 4°.

The tests were conducted in the Langley 4- by 4-foot supersonic pressure tunnel which is described in reference 13.

TESTS

Test Conditions

The conditions for the tests were:

Mach number	1.61	2.01
Reynolds number, based on the wing M.A.C.	1.90×10^6	1.52×10^6
Stagnation dewpoint, °F	-20	-25
Stagnation pressure, lb/sq in.	15	14
Stagnation temperature, °F	110	110

The magnitudes of the variations in the test-section flow parameters for the two test Mach numbers were:

Mach number variation	±0.01	±0.015
Flow angle in the horizontal or vertical plane, deg	±0.1	±0.1

CORRECTIONS AND ACCURACY

The angles of attack and sideslip were corrected for the deflection of the balance and sting under load. No corrections were applied to the data for the flow variations in the test section.

The estimated errors in the data are:

C_L	±0.003
C_X	±0.001
C_Y	±0.001
C_m	±0.0006
C_n	±0.0003
C_l	±0.0003
α, deg	±0.1
β, deg	±0.1
δ_r, deg	±0.1
i_t, deg	±0.1

The base pressure was measured and the longitudinal-force data were corrected to a base pressure equal to free-stream static pressure.

RESULTS AND DISCUSSION

The experimental variations with sideslip angle of C_n, C_l, and C_Y are presented in figure 6 for $M = 1.61$ and figure 7 for $M = 2.01$. Also shown in figures 6 and 7 are the theoretical estimates of these coefficients for the complete model (ref. 5) and calculated values of the body-alone lateral-force and yawing-moment coefficients (ref. 12).

All wing-on configurations tested had the wing fences installed with the exception of the complete model at $M = 2.01$ and $\alpha = 0^\circ$. The negligible effect of the wing fences is indicated in figure 8.

Values of the stability derivatives C_{Y_β}, C_{l_β}, and C_{n_β} measured from the results shown in figures 6 and 7 are presented in table IV.

The results shown in figures 6 and 7 indicate, as could be expected, that the largest contribution to C_Y comes from the vertical tail, with small changes due to addition of the wing or deflection of the rudder. Theoretical estimates agree well with the experimental results for the complete model but are somewhat low for the body alone. There was little change in C_{Y_β} for the complete airplane at the two test Mach numbers (table IV).

At zero angle of attack C_l is almost entirely due to the vertical tail. At $\alpha = 4^\circ$ the wing has a substantial contribution, which was expected. Theoretical estimates are somewhat low. The effective dihedral C_{l_β} of the complete airplane was but slightly changed between the two test Mach numbers (table IV).

At zero angle of attack the stabilizing portion of C_n is almost entirely due to the vertical tail. At $\alpha = 4^\circ$ the small stabilizing wing contribution increased slightly, as was expected. Theoretical estimates of the unstable body moment agree well with the experimental results, but the estimates of the tail contribution seem to be somewhat high. The change in C_{n_β} for the complete airplane was small between the test Mach numbers (table IV). At $\alpha = 0^\circ$ the variation of C_n with β is linear at $M = 2.01$ but not at $M = 1.61$ (figs. 6 and 7). As a result, the measured values of C_{n_β} for a small β range at $M = 1.61$ inadequately describe the variation of C_n with β.

The longitudinal forces and moments corresponding to the lateral forces and moments of figures 6 and 7 are presented in figures 9 and 10. There are no significant changes in the coefficients with sideslip angle apparent from figures 9 and 10, with the possible exception of the pitching-moment coefficient. For the complete model near the trim condition, however, the pitching-moment coefficient remains essentially constant at sideslip angles less than about 6°.

A comparison of the theoretical, flight, and wind-tunnel values of the static-directional-stability derivative C_{n_β} is given in figure 11. It is shown in the figure that the experimental body-alone C_{n_β} is essentially constant with Mach number and is close to the theoretical value. The addition of the wing has a small stabilizing effect which gives the wing-body combination a constant contribution. In the case of the complete configuration, however, there are significant differences in the theoretical, flight, and wind-tunnel values. Theory indicates a large contribution of the vertical tail which decreases somewhat with increasing Mach number. The wind-tunnel results indicate a slightly smaller contribution which is essentially constant. Flight results, on the other hand, indicate a large tail contribution which decreases very rapidly with Mach number. The values of C_{n_β} for Mach numbers greater than 1.7 reported from an analysis of flight-test results are somewhat lower than the wind-tunnel values. As explained in reference 11, however, there is some doubt as to the reliability of the one-dimensional analysis of the flight-test data because of the large rolling motion which occurred during the high-speed flights. For detailed discussion of the flight results, reference 11 should be consulted. Since the vertical tail of the test model was smaller than that on a 1/16-scale model of the airplane (fig.4), the values of C_{n_β} for the complete model from the tunnel tests are conservative. Tunnel tests at other Mach numbers are needed to establish the real trend of C_{n_β} with Mach number.

The variation of C_Y, C_n, and C_l with C_L for sideslip angles of 0° and -4° shown in figure 12 was used to determine the variation of C_{Y_β}, C_{n_β}, and C_{l_β} with C_L presented in figure 13. Values of C_{Y_β}, C_{n_β}, and C_{l_β} from table IV are shown for comparison. These slopes are not in exact agreement with those obtained from figure 12 because of the nonlinear variation of C_Y, C_n, and C_l with β. The values of C_{Y_β}, C_{n_β}, and C_{l_β} shown in figure 13 should, however, indicate the probable variation through the lift range of the present investigation.

The directional control characteristics are presented in figure 14 for $\alpha = 0^\circ$ and 4° for Mach numbers of 1.61 and 2.01. The theoretical variation of C_n with δ_r obtained by the method of reference 14 is also shown. Although the calculated values of $C_{n_{\delta_r}}$ are somewhat higher than the experimental values, the predicted decrease in $C_{n_{\delta_r}}$ at the higher Mach number is indicated by the experimental results. The effect of angle of attack on $C_{n_{\delta_r}}$ appears to be negligible. There is a slight increase in the value of β_{δ_r} with increasing α at $M = 1.61$, but at $M = 2.01$ the value of β_{δ_r} is greater at $\alpha = 4^{\circ}$ because of the decrease in C_{n_β} at this angle of attack. At both angles of attack the values of C_{n_β} are smaller at $M = 2.01$ than at $M = 1.61$.

The effect of the wing on the vertical-tail contribution to the lateral characteristics is shown in figure 15. Vertical-tail increments $\left(\Delta C_Y\right)_t$, $\left(\Delta C_l\right)_t$, and $\left(\Delta C_n\right)_t$ were obtained from the data presented in figures 6 and 7 by measuring the differences between the tail-on and tail-off results for configurations with and without the wing. Addition of the wing reduced the values of $\left(\Delta C_Y\right)_t$ and $\left(\Delta C_n\right)_t$ and increased slightly the values of $\left(\Delta C_l\right)_t$.

CONCLUDING REMARKS

Results of tests of a 1/16-scale model of the Douglas D-558-II research airplane in the Langley 4- by 4-foot supersonic pressure tunnel at Mach numbers of 1.61 and 2.01 indicate that the complete model has positive directional stability and positive effective dihedral at both Mach numbers. The apparent differences in trend between flight- and tunnel-test results are believed to be due to the difficulty experienced in measuring the directional-stability derivative C_{n_β} in flight during combined rolling and yawing motions.

The stabilizing forces and moments are contributed almost entirely by the tail, but a small reduction in the stabilizing side force and yawing moment is due to the addition of the wing. Addition of the wing increases the contribution to the rolling moment contributed by the vertical tail.

Rudder effectiveness was less at the higher Mach number as indicated by linear theory.

Langley Aeronautical Laboratory,
National Advisory Committee for Aeronautics,
Langley Field, Va., September 11, 1953.

REFERENCES

1. Kerker, R., and Miller, C. E.: Summary Report of Model D-558-2 Tests at Cooperative Wind Tunnel. Rep. No. ES-20648, Douglas Aircraft Co., Inc., Oct. 1, 1946.

2. Osborne, Robert S.: High-Speed Wind-Tunnel Investigation of the Longitudinal Stability and Control Characteristics of a 1/16-Scale Model of the D-558-2 Research Airplane at High Subsonic Mach Numbers and at a Mach Number of 1.2. NACA RM L9C04, 1949.

3. Spearman, M. Leroy: Static Longitudinal Stability and Control Characteristics of a 1/16-Scale Model of the Douglas D-558-II Research Airplane at Mach Numbers of 1.61 and 2.01. NACA RM L53I22, 1953.

4. Queijo, M. J., and Michael, W. H., Jr.: Analysis of the Effects of Various Mass, Aerodynamic, and Dimensional Parameters on the Dynamic Lateral Stability of the Douglas D-558-2 Airplane. NACA RM L9A24, 1949.

5. Queijo, M. J., and Goodman, Alex: Calculations of the Dynamic Lateral Stability Characteristics of the Douglas D-558-II Airplane in High-Speed Flight for Various Wing Loadings and Altitudes. NACA RM L50H16a, 1950.

6. Sjoberg, Sigurd A.: Preliminary Measurements of the Dynamic Lateral Stability Characteristics of the Douglas D-558-II (BuAero No. 37974) Airplane. NACA RM L9G18, 1949.

7. Sjoberg, S. A.: Flight Measurements with the Douglas D-558-II (BuAero No. 37974) Research Airplane. Static Lateral and Directional Stability Characteristics as Measured in Sideslips at Mach Numbers up to 0.87. NACA RM L50C14, 1950.

8. Stillwell, W. H., and Wilmerding, J. V.: Flight Measurements With the Douglas D-558-II (BuAero No. 37974) Research Airplane. Dynamic Lateral Stability. NACA RM L51C23, 1951.

9. Just, T. R., and Carder, A. B.: D558-II Flight Test Status Report for Week Ending 11 August 1951. Rep. No. Dev-752, Sev. No. 51-32, Douglas Aircraft Co., Inc., Aug. 16, 1951.

10. Williams W. C., and Crossfield, A. S.: Handling Qualities of High-Speed Airplanes. NACA RM L52A08, 1952.

11. Ankenbruck, Herman O., and Dahlen, Theodore E.: Some Measurements of Flying Qualities of a Douglas D-558-II Research Airplane During Flights to Supersonic Speeds. RM L53A06, 1953.

12. Allen, H. Julian: Estimation of the Forces and Moments Acting on Inclined Bodies of Revolution of High Fineness Ratio. NACA RM A9I26, 1949.

13. Robinson, Ross B., and Driver, Cornelius: Aerodynamic Characteristics at Supersonic Speeds of a Series of Wing-Body Combinations Having Cambered Wings With an Aspect Ratio of 3.5 and a Taper Ratio of 0.2 - Effects of Sweep Angle and Thickness Ratio on the Aerodynamic Characteristics in Pitch at $M = 1.60$. NACA RM L51K16a, 1952.

14. Kainer, Julian H., and Marte, Jack E.: Theoretical Supersonic Characteristics of Inboard Trailing-Edge Flaps Having Arbitrary Sweep and Taper. Mach Lines Behind Flap Leading and Trailing Edges. NACA TN 2205, 1950.

TABLE I

DIMENSIONS OF THE 1/16-SCALE MODEL OF THE

DOUGLAS D-558-II RESEARCH AIRPLANE

Wing:	
Root airfoil section (normal to 0.30 chord of unswept panel)	NACA 63-010
Tip airfoil section (normal to 0.30 chord of unswept panel)	NACA 63-010
Total area (including fuselage intercept) sq ft	0.684
Span, in.	18.72
Mean aerodynamic chord, in.	5.46
Root chord (parallel to plane of symmetry), in.	6.78
Tip chord (parallel to plane of symmetry), in.	3.83
Taper ratio	0.565
Aspect ratio	3.57
Sweep of 0.30-chord line of unswept panel, deg	35
Incidence of fuselage center line, deg	3
Dihedral, deg	-3
Geometric twist, deg	0
Horizontal tail:	
Root airfoil section (normal to 0.30 chord of unswept panel)	NACA 63-010
Tip airfoil section (normal to 0.30 chord of unswept panel)	NACA 63-010
Area (including fuselage intercept), sq ft	0.156
Span, in.	8.98
Mean aerodynamic chord, in.	2.61
Root chord (parallel to plane of symmetry), in.	3.35
Tip chord (parallel to plane of symmetry), in.	1.68
Taper ratio	0.50
Aspect ratio	3.59
Sweep of 0.30-chord line of unswept panel, deg	40
Dihedral, deg	0
Elevator area, sq ft	0.059
Vertical tail:	
Airfoil section (parallel to fuselage center line)	NACA 63-010
Area (leading edge and trailing edge extended to fuselage center line), sq ft	0.215
Span (from fuselage center line), in.	5.25
Root chord (parallel to fuselage center line), in.	9.14
Tip chord (parallel to fuselage center line), in.	2.75
Sweep of 0.30-chord line of unswept panel, deg	49
Rudder area, sq ft	0.030

TABLE I.- Concluded.

DIMENSIONS OF THE 1/16-SCALE MODEL OF THE

DOUGLAS D-558-II RESEARCH AIRPLANE

Fuselage:	
Length, in.	31.50
Maximum diameter, in.	3.75
Fineness ratio	8.40
Base diameter, in.	1.56

TABLE II

COORDINATES OF THE BODY

[x is distance along model center line from the nose of the model; r is the radius; all dimensions in inches.]

x	r
0	0
1.000	.382
2.000	.719
3.000	1.010
4.000	1.256
5.000	1.457
6.000	1.614
7.000	1.729
8.000	1.806
9.000	1.851
10.000	1.871
11.000	1.875
16.250	1.875
17.000	1.872
18.000	1.858
19.000	1.833
20.000	1.794
21.000	1.743
22.000	1.679
23.000	1.602
24.000	1.513
24.297	1.485
31.500	.780

TABLE III

COORDINATES OF WING FENCES AND AIRFOIL SECTION IN THE PLANE OF THE FENCES

[x is distance from the leading edge along center line of airfoil section; y is distance perpendicular to center line (see fig. 3); all dimensions in inches.]

Airfoil section		Fence	
x	y	x	y
0	0	-----	-----
.334	.128	0.334	0.128
.955	.207	.955	.585
1.672	.249	1.672	.746
2.259	.259	2.259	.766
3.073	.219	3.073	.687
4.155	.125	4.155	.125
5.59	0	-----	-----

TABLE IV

LATERAL-STATIC-STABILITY DERIVATIVES FOR THE VARIOUS CONFIGURATIONS OF THE 1/16-SCALE MODEL OF THE D-558-II RESEARCH AIRPLANE

$[-2^{\circ} \geqq \beta \geqq 2^{\circ}]$

Configuration	δ_r, deg	α, deg	M = 1.61			M = 2.01		
			C_{n_β}	C_{l_β}	C_{Y_β}	C_{n_β}	C_{l_β}	C_{Y_β}
Body	--	0	-0.0041	0	-0.0016	-0.0043	0	-0.0036
Body-wing	--	0	-.0036	.0001	-.0040	-.0036	0	-.0047
Body-vertical-tail	0	0	.0022	-.0015	-.0137	.0016	-.0012	-.0125
Complete model	0	0	.0016	-.0013	-.0126	.0020	-.0014	-.0125
	-2.2	0	.0016	-.0012	-.0123	.0019	-.0014	-.0125
	-4.0	0	.0016	-.0012	-.0130	.0019	-.0015	-.0132
Body-wing	--	4	-.0030	-.0003	-.0050	-.0031	-.0004	-.0055
Body-vertical-tail	0	4	.0020	-.0010	-.0120	.0012	-.0010	-.0115
Complete model	0	4	.0018	-.0011	-.0128	.0015	-.0013	-.0133
	-2.2	4	--------	------	--------	.0015	-.0013	-.0135
	-4.0	4	--------	------	--------	.0015	-.0013	-.0137

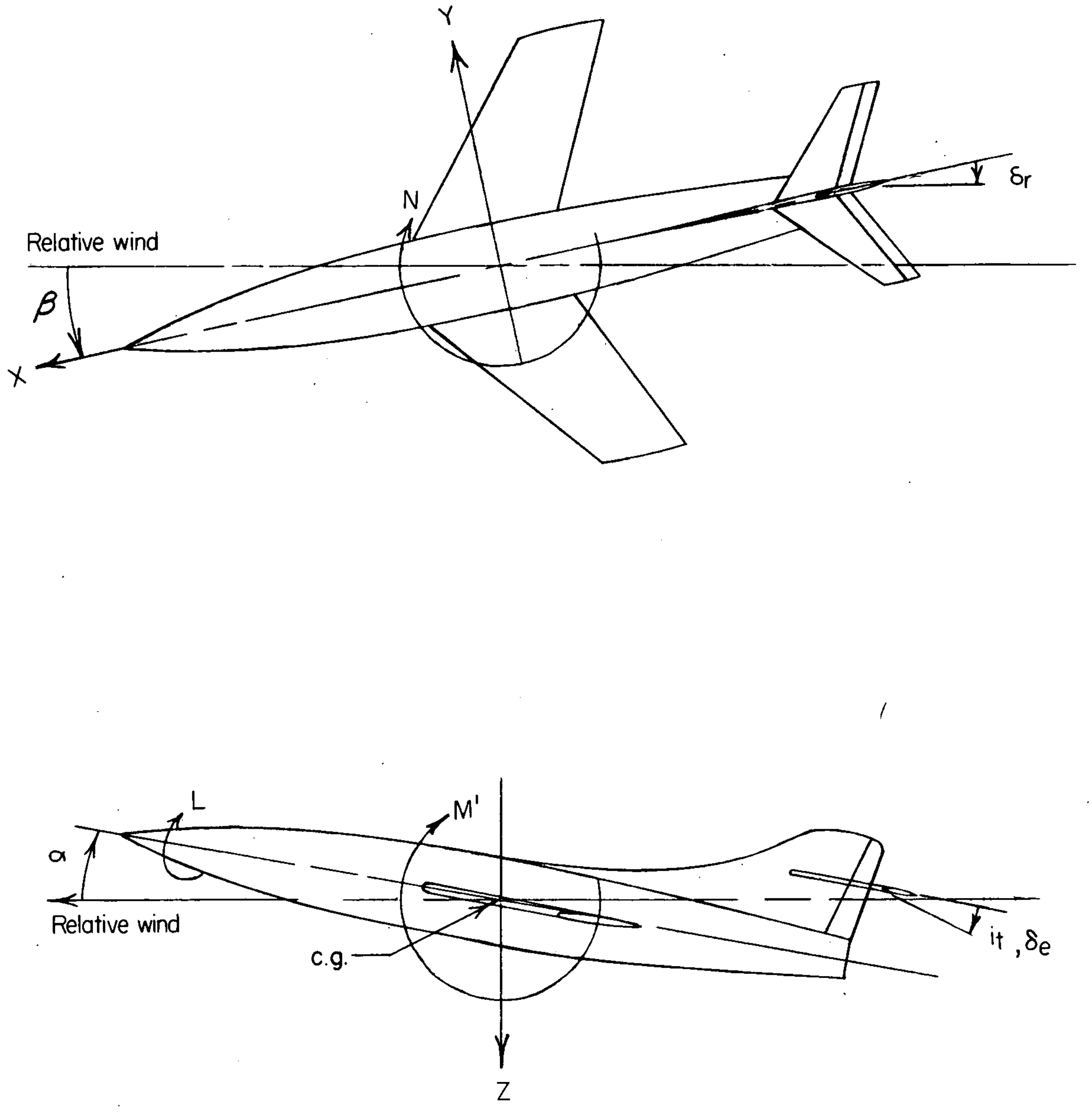

Figure 1.- System of stability axes. Arrows indicate positive values.

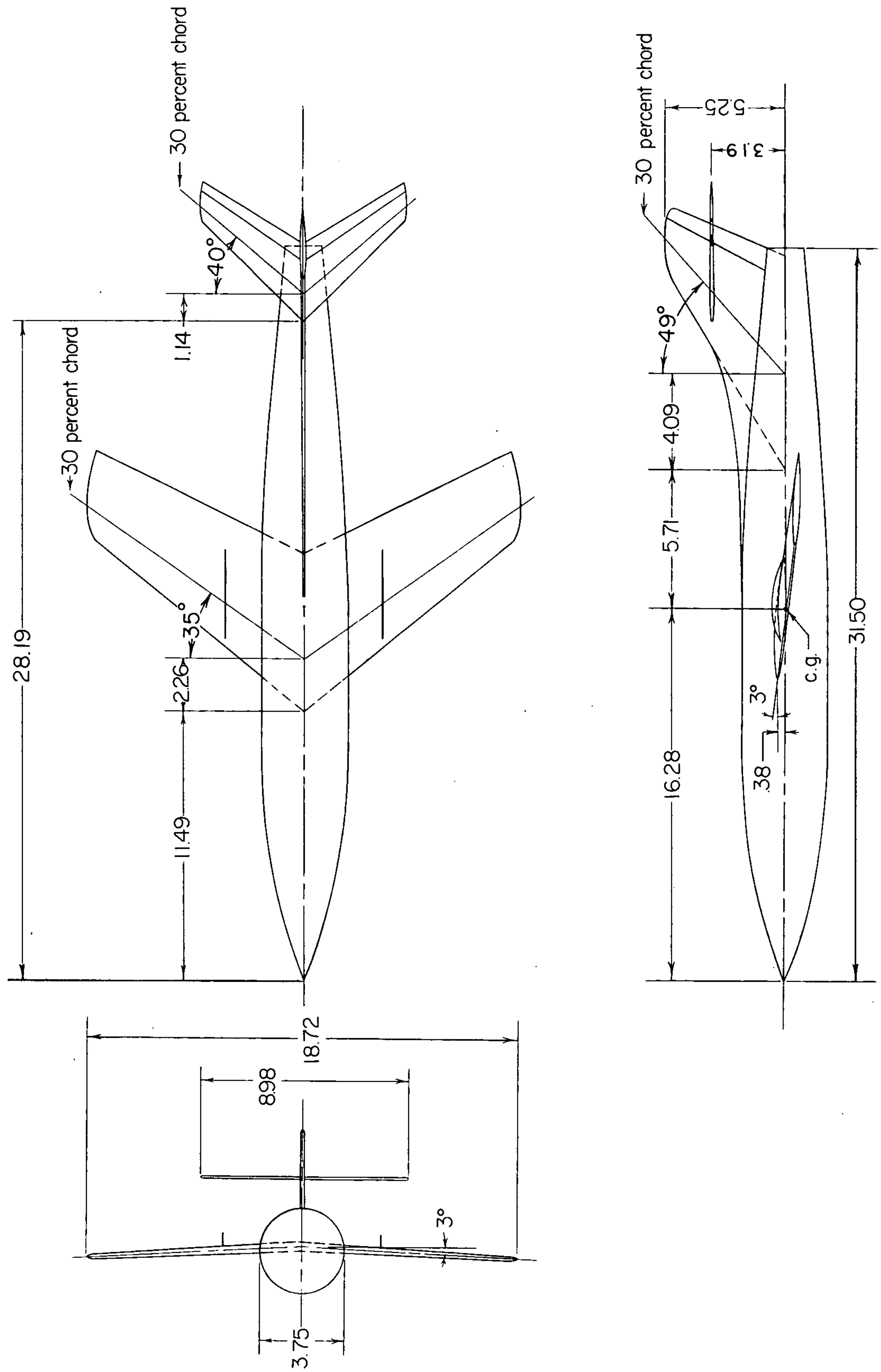

Figure 2.- Details of model. All dimensions in inches, unless otherwise noted.

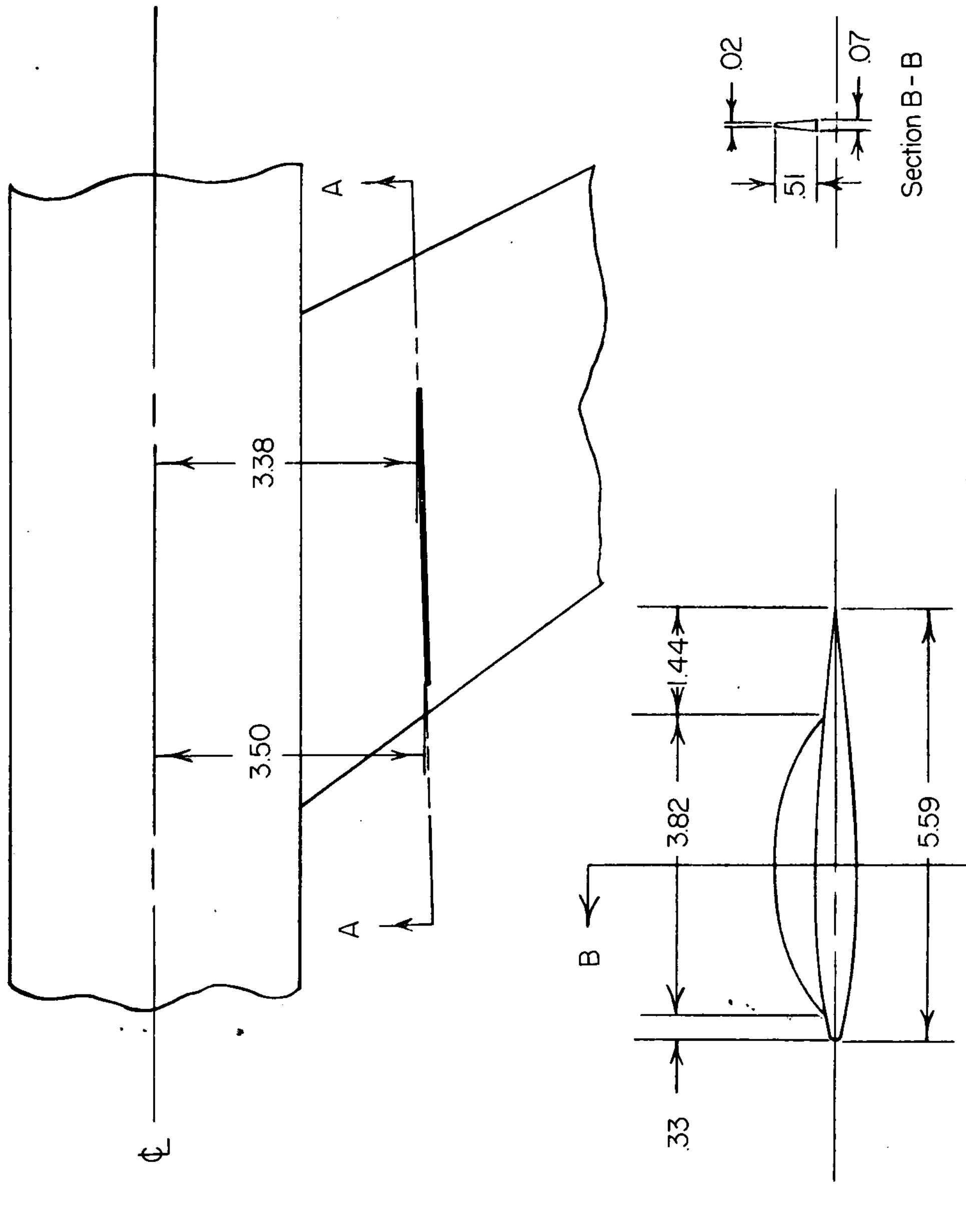

Figure 3.- Wing-fence details. All dimensions in inches.

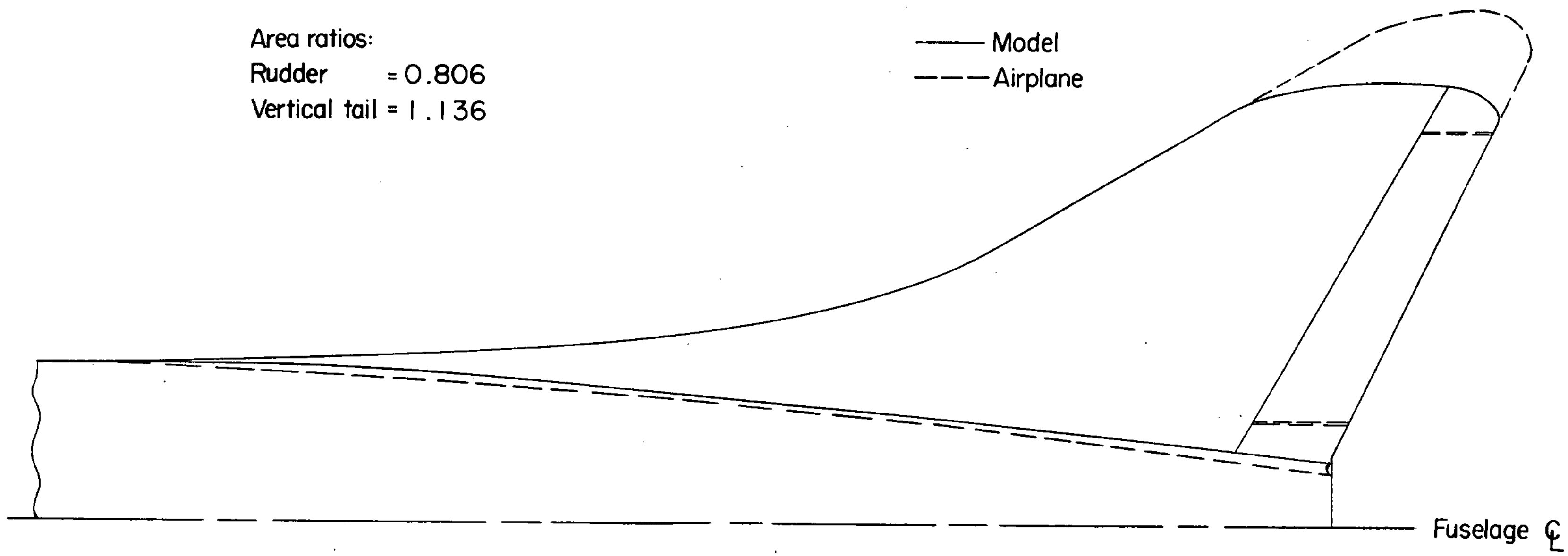

Figure 4.- Vertical-tail configurations of model and airplane. Vertical-tail area ratio based on exposed area.

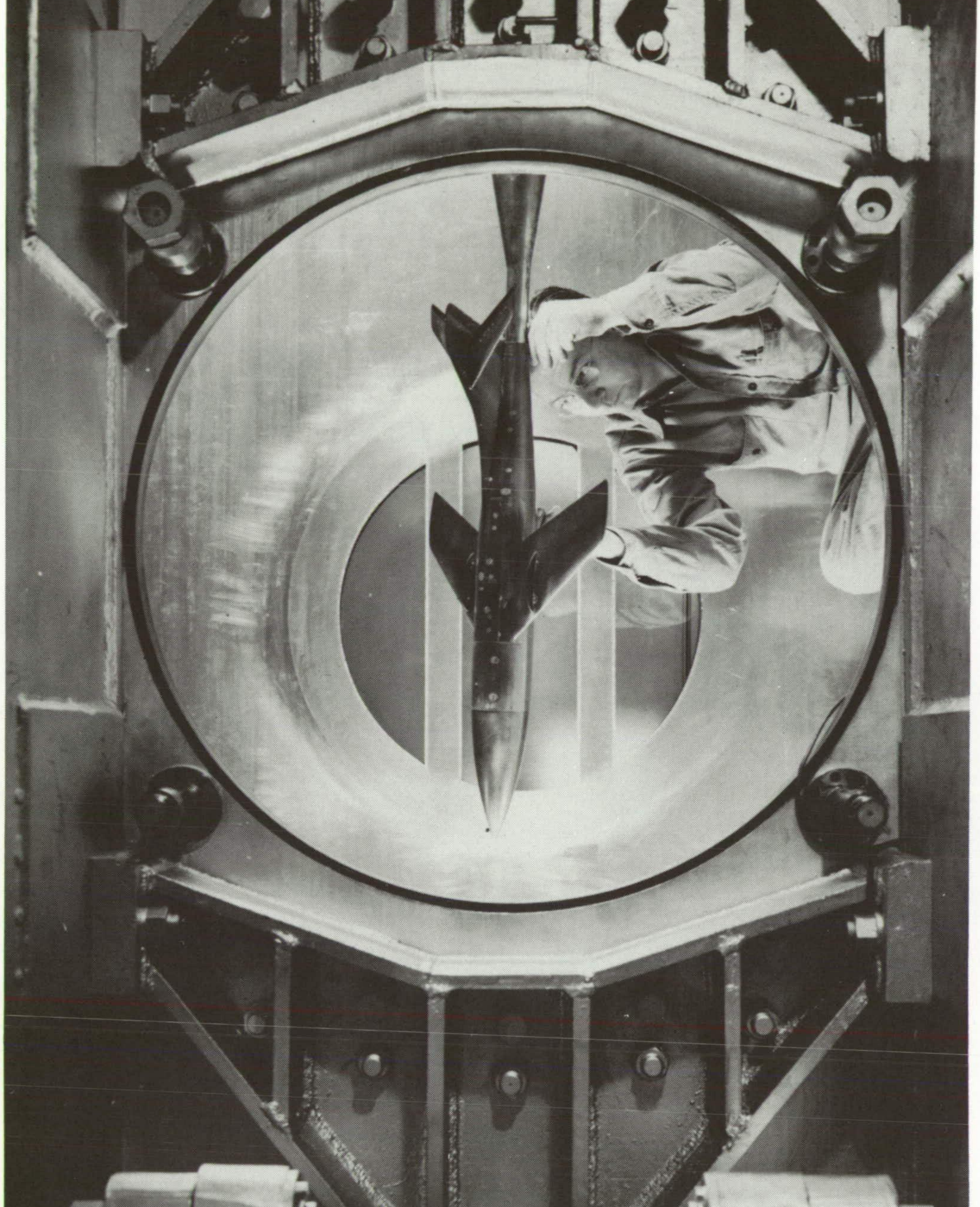

L-74802

Figure 5.- Installation of model in test section.

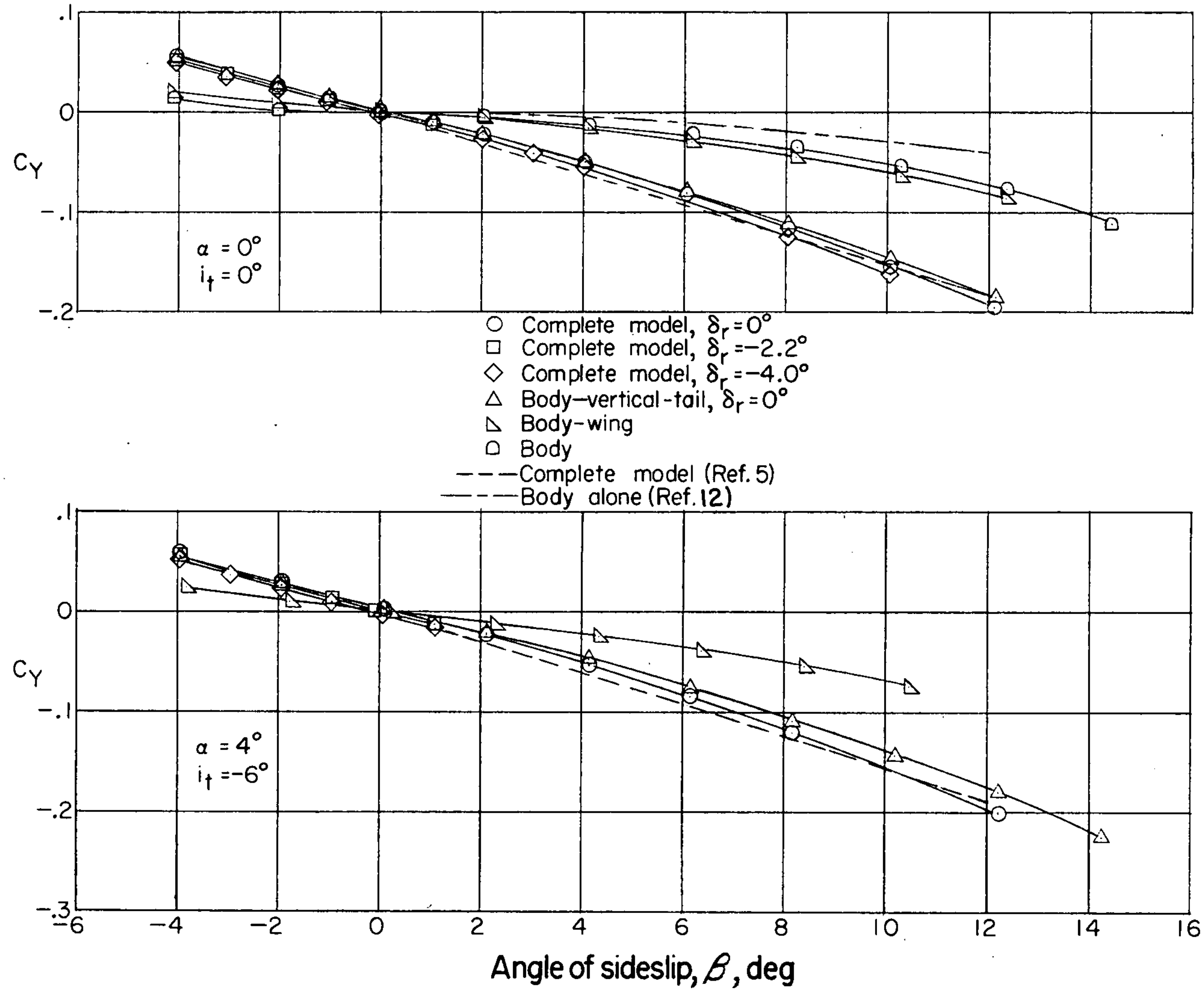

Figure 6.- Variation of lateral-force, rolling-moment, and yawing-moment coefficients with sideslip angle for the various configurations. M = 1.61.

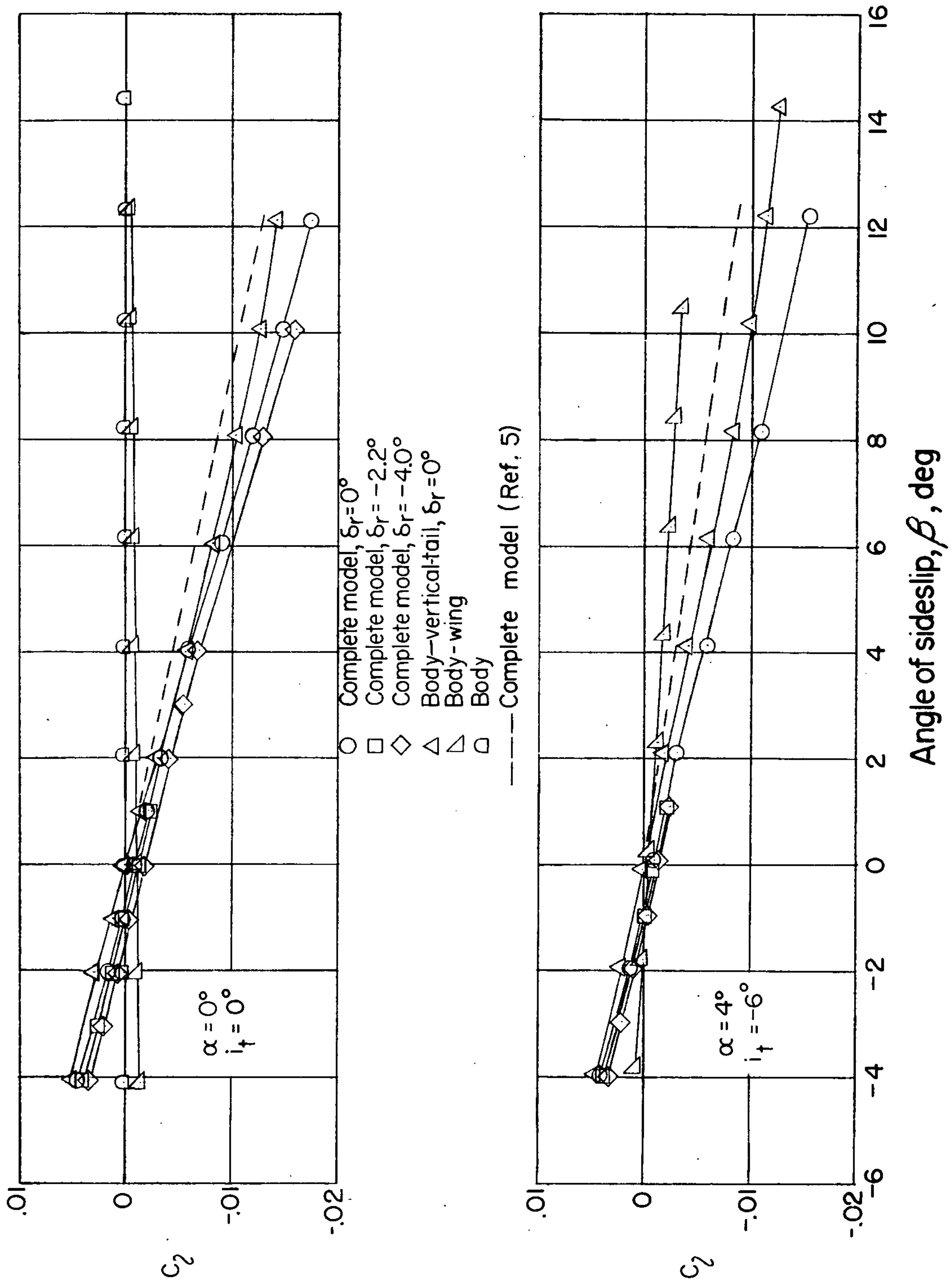

Figure 6.- Continued.

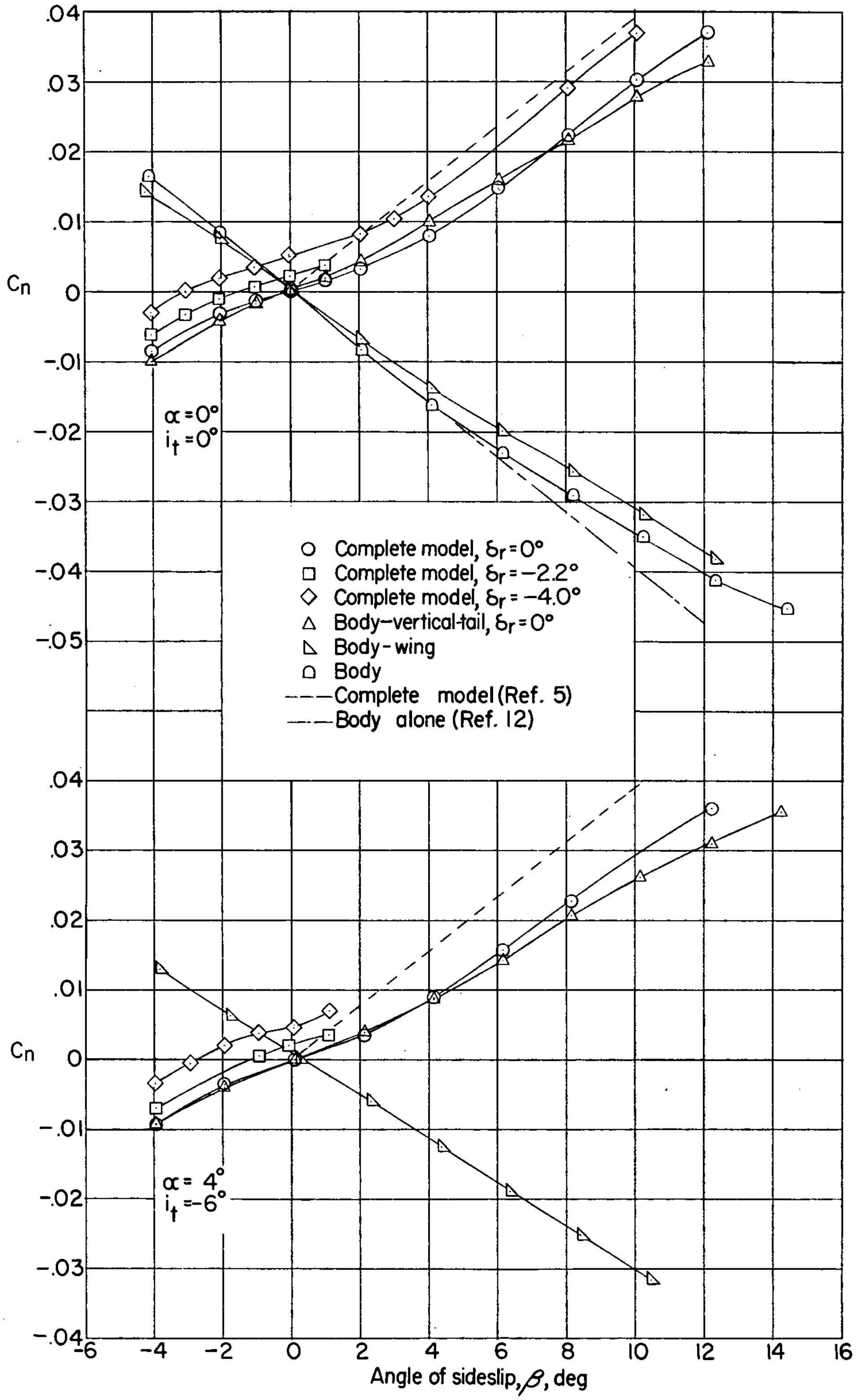

Figure 6.- Concluded.

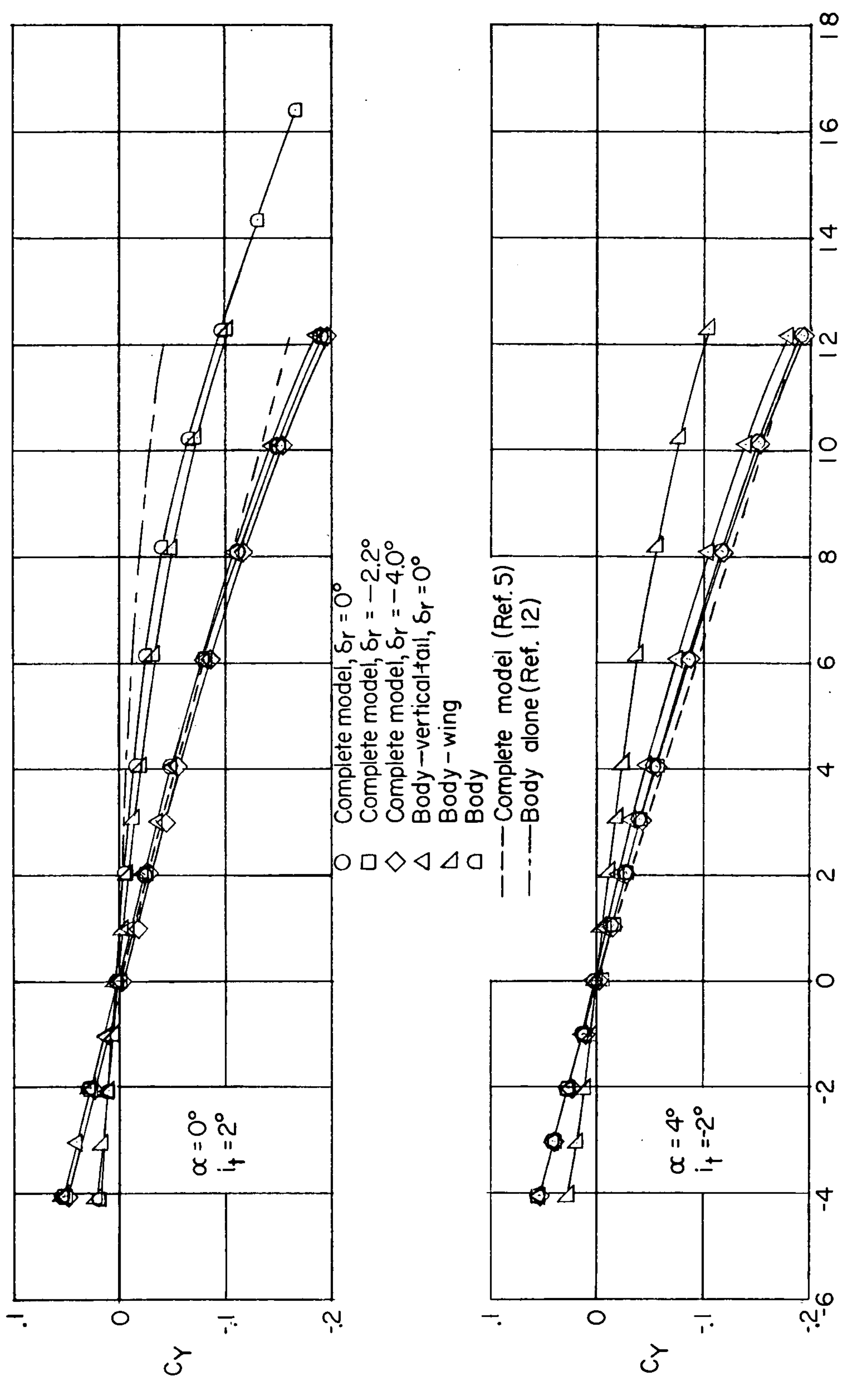

Figure 7.- Variation of lateral-force, rolling-moment, and yawing-moment coefficients with sideslip angle for the various configurations. M = 2.01.

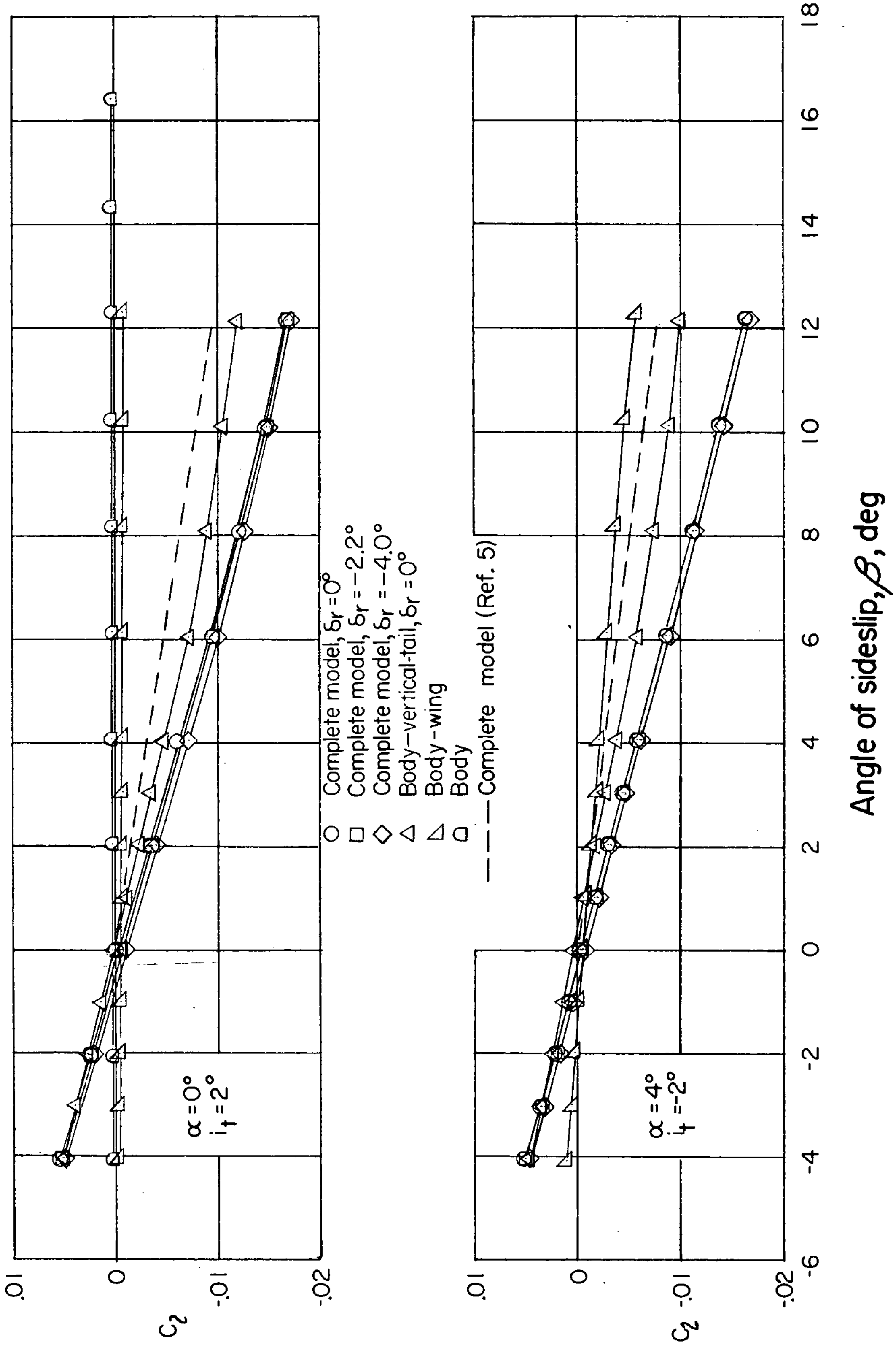

Figure 7.- Continued.

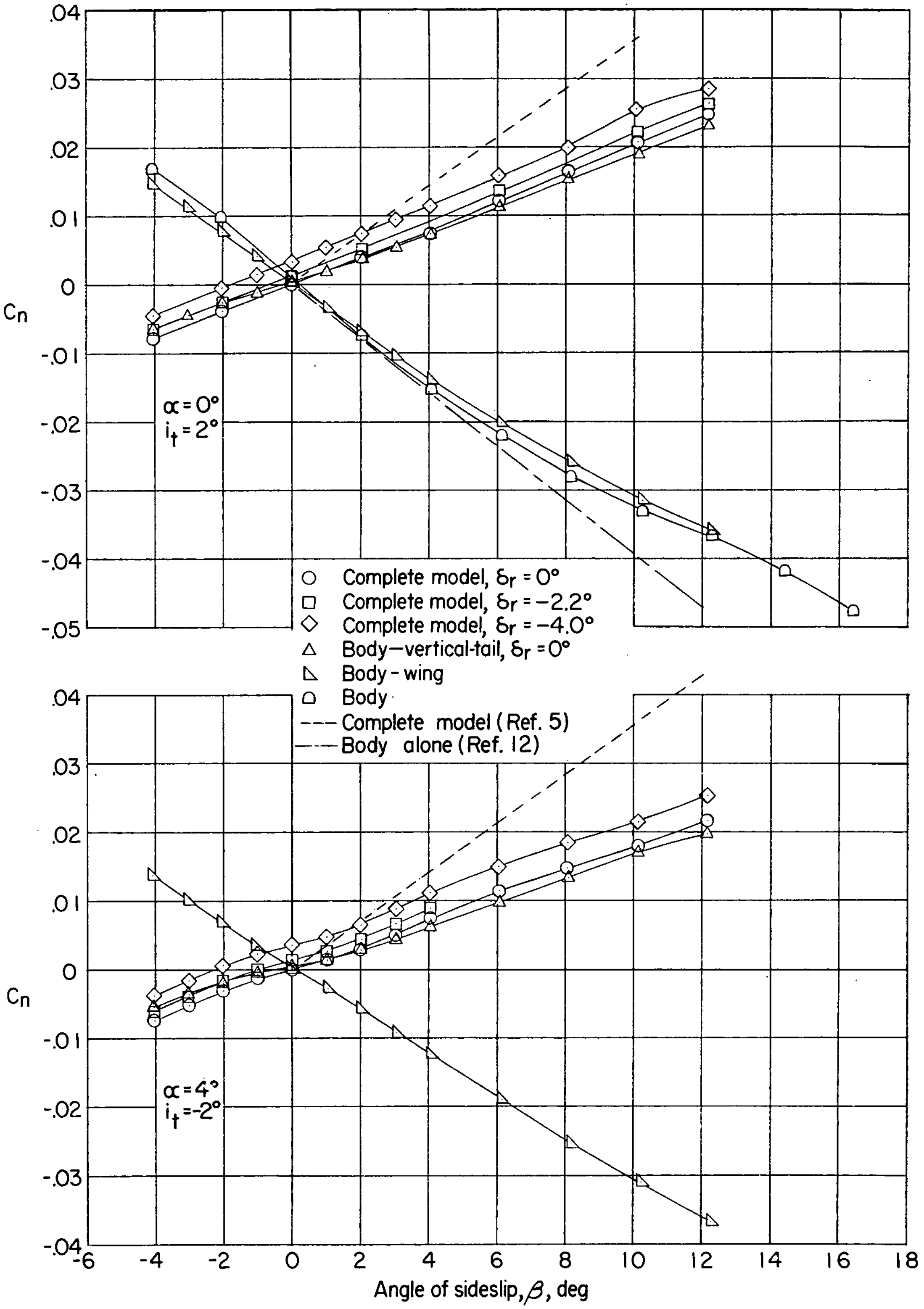

Figure 7.- Concluded.

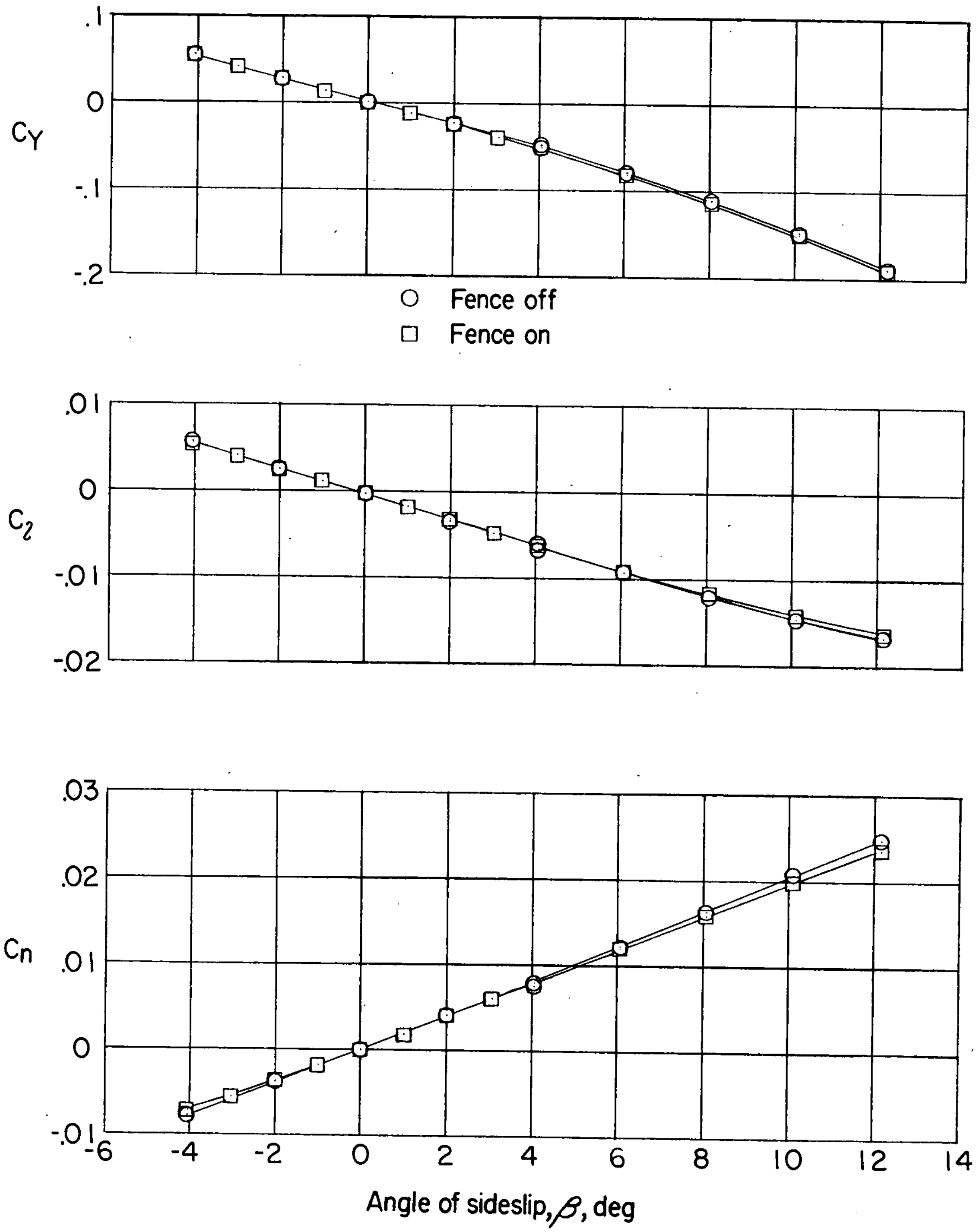

Figure 8.- Effect of the addition of wing fences on the aerodynamic characteristics in sideslip. Complete model; $M = 2.01$; $\alpha = 0^{\circ}$; $\delta_r = 0^{\circ}$; $i_t = 2^{\circ}$.

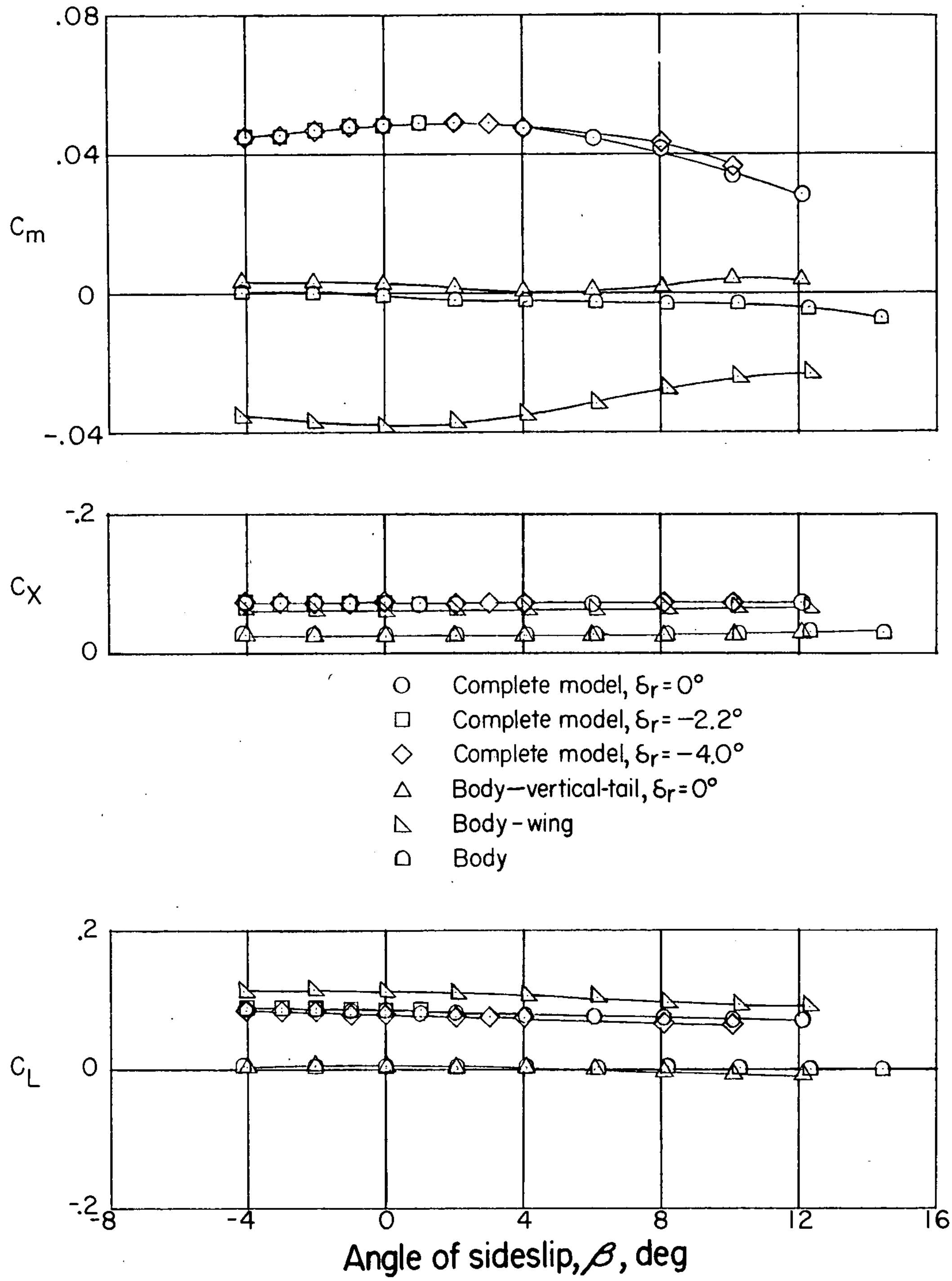

(a) $\alpha = 0°$; $i_t = 0°$.

Figure 9.- Variation of longitudinal-force, pitching-moment, and lift coefficients with sideslip angle for the various configurations. M = 1.61.

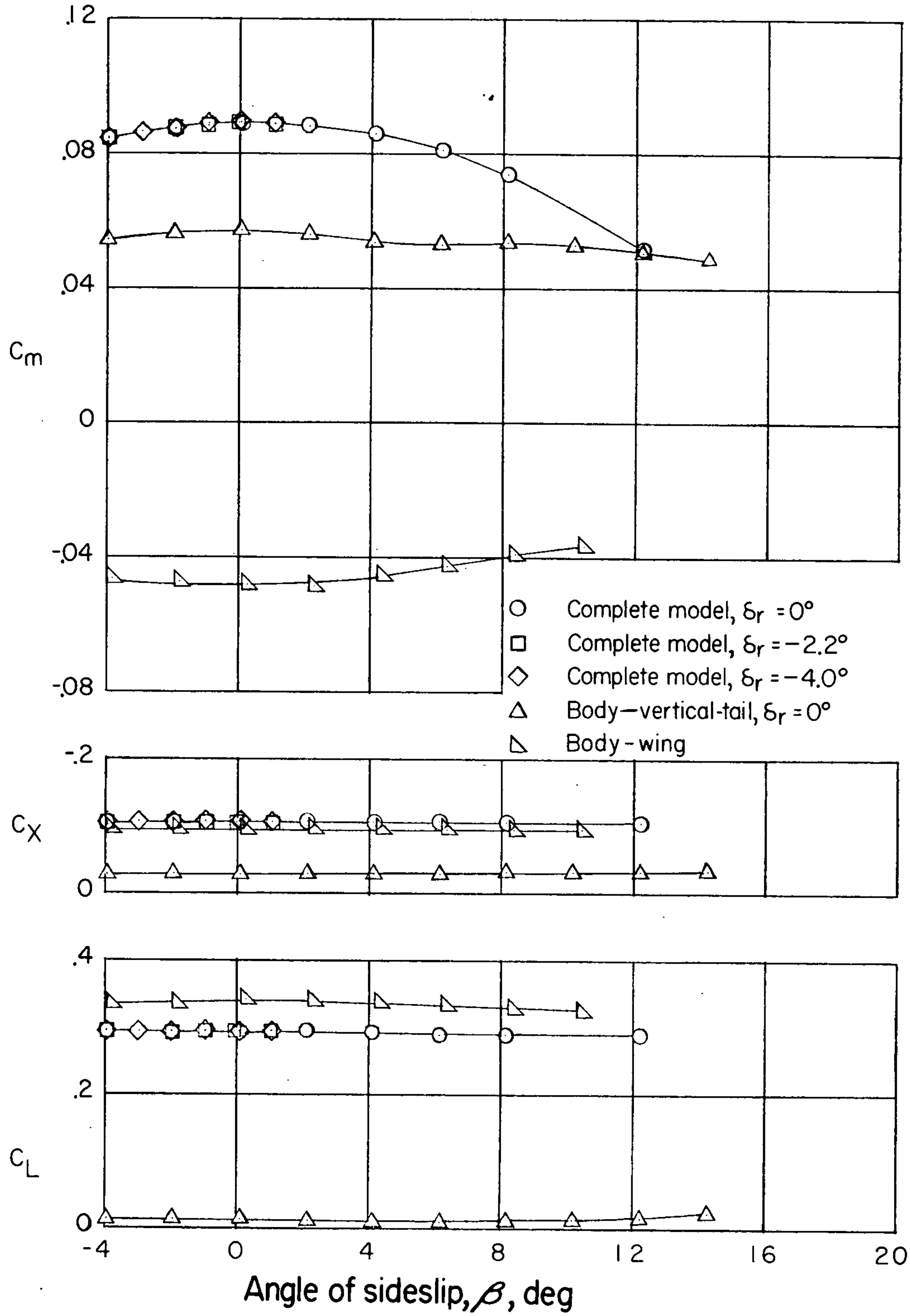

(b) $\alpha = 4°$; $i_t = -6°$.

Figure 9.- Concluded.

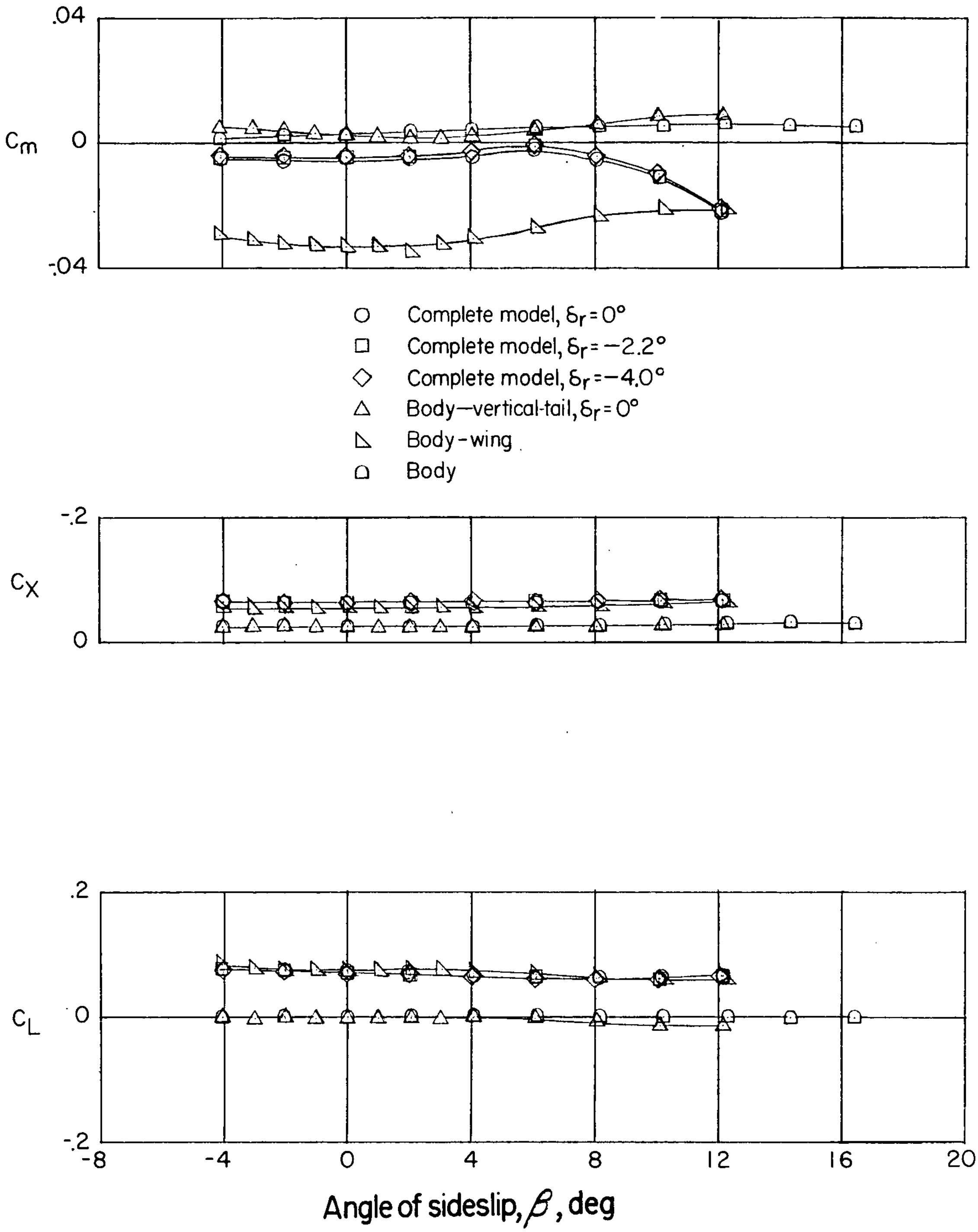

(a) $\alpha = 0^{\circ}$; $i_t = 2^{\circ}$.

Figure 10.- Variation of longitudinal-force, pitching-moment, and lift coefficients with sideslip angle for the various configurations. M = 2.01.

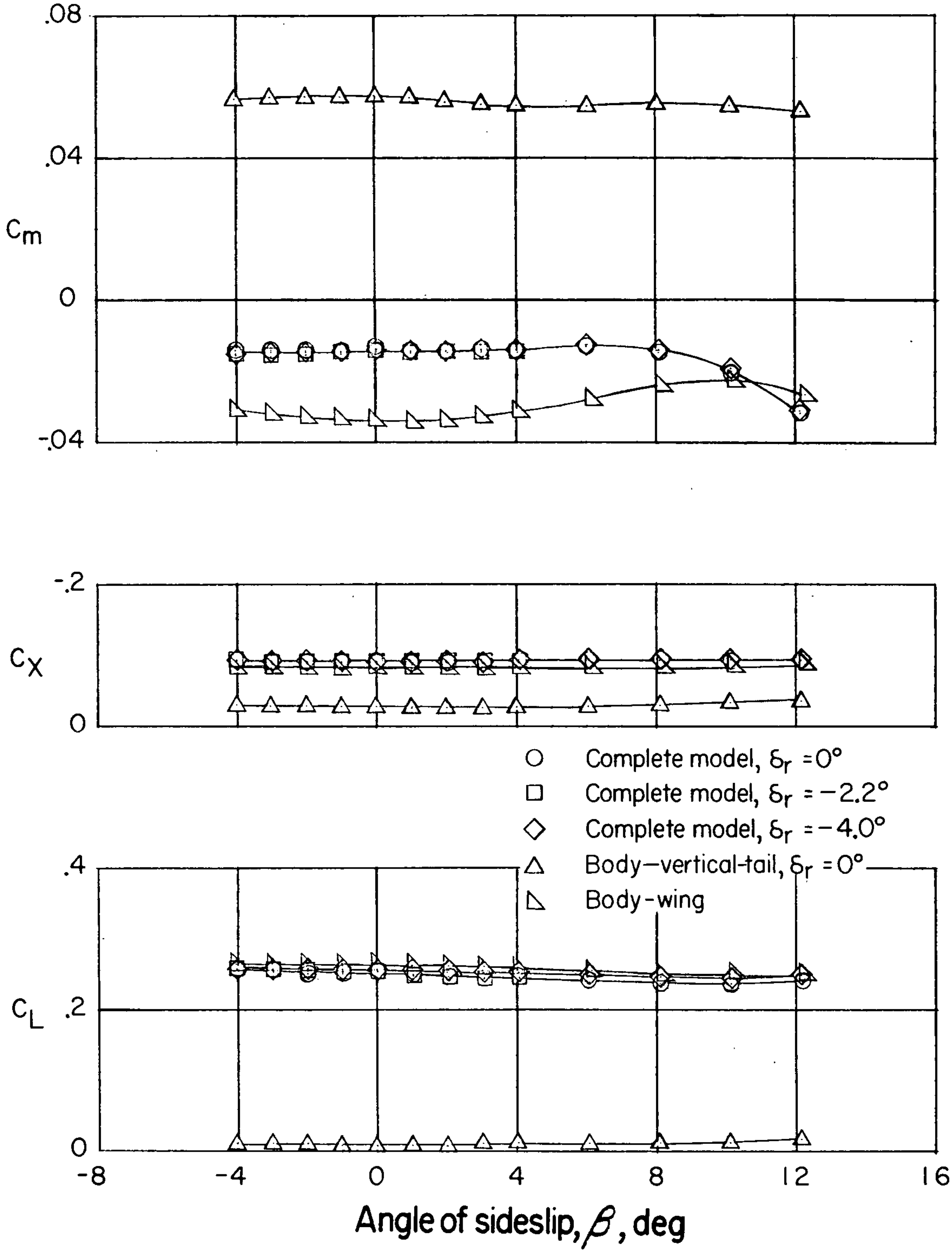

(b) $\alpha = 4^{\circ}$; $i_t = -2^{\circ}$.

Figure 10.- Concluded.

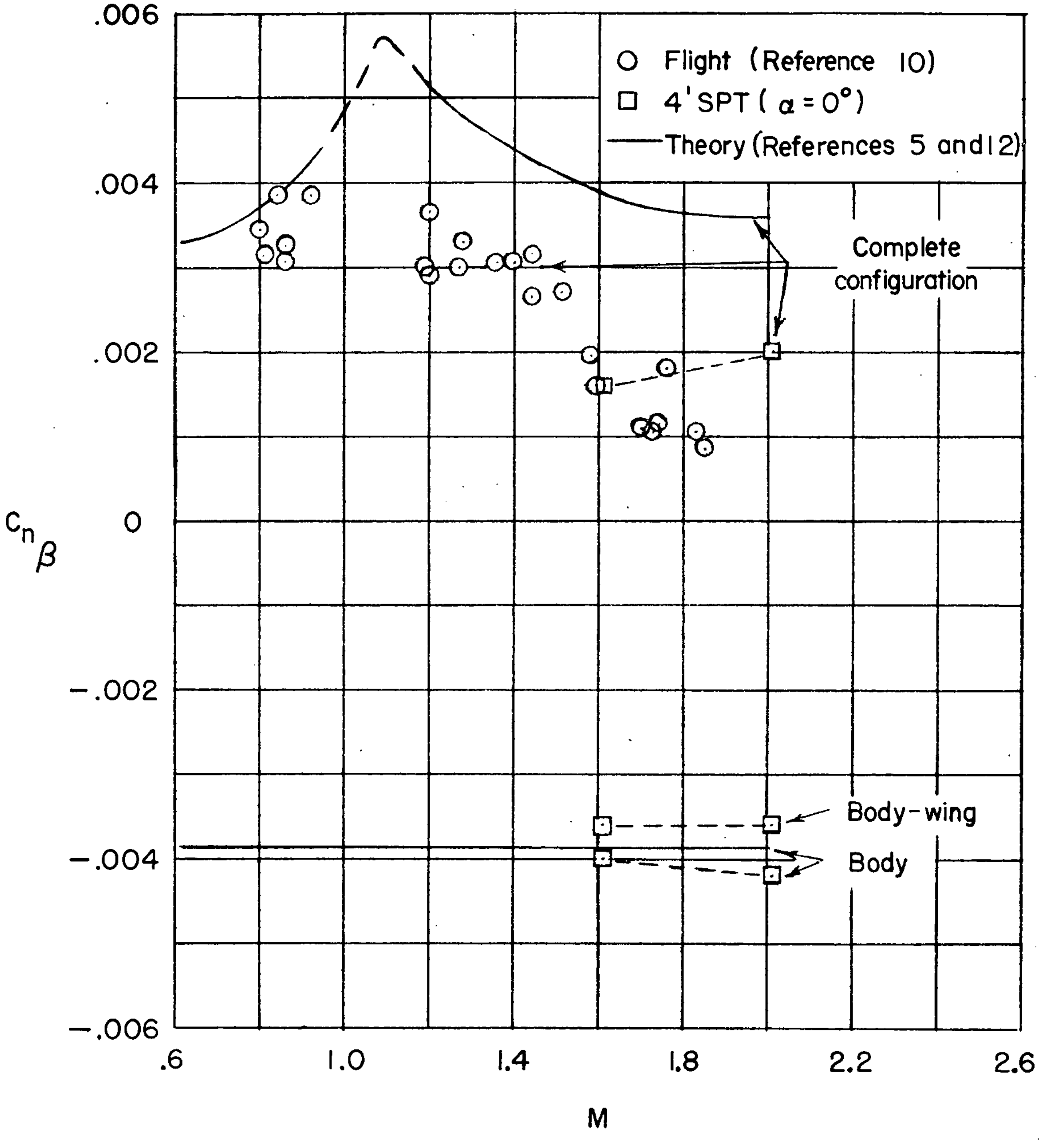

Figure 11.- Variation with Mach number of the static-directional-stability derivative derived from theory, flight tests, and wind-tunnel tests.

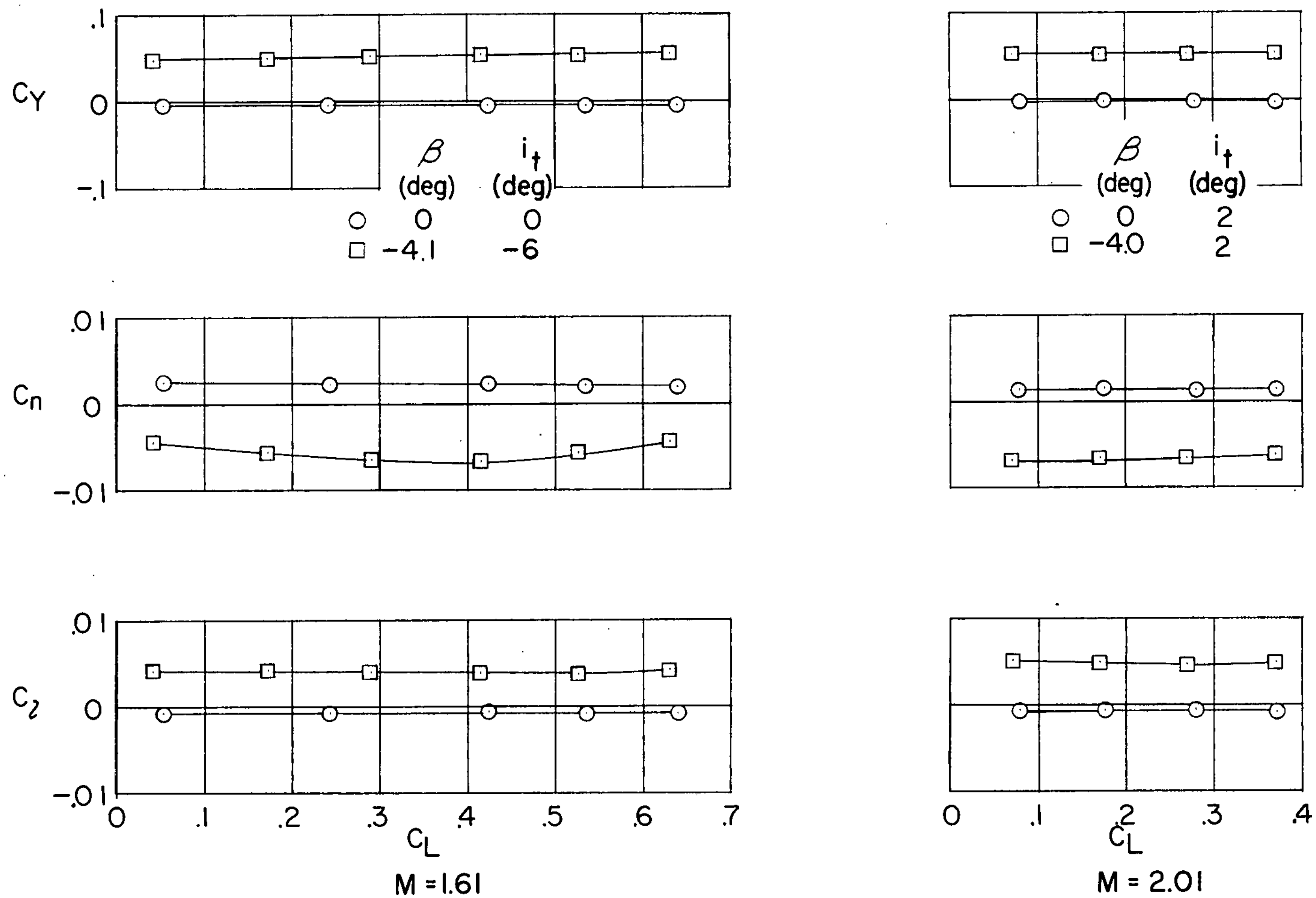

(a) Lateral characteristics.

Figure 12.- Variation with lift coefficient of the lateral characteristics and the angle of attack. Complete model; $\delta_r = 0^{\circ}$.

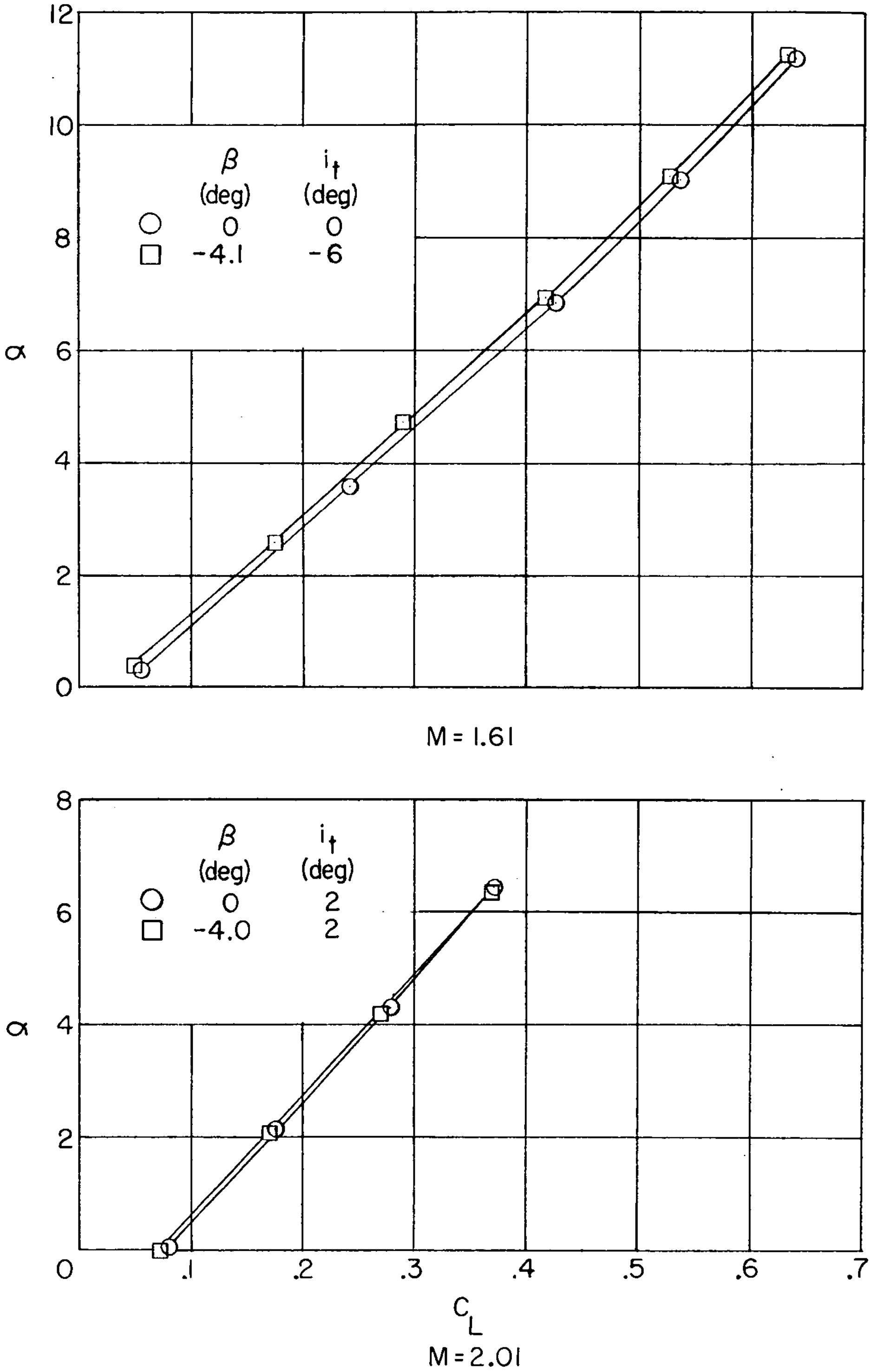

(b) Angle of attack.

Figure 12.- Concluded.

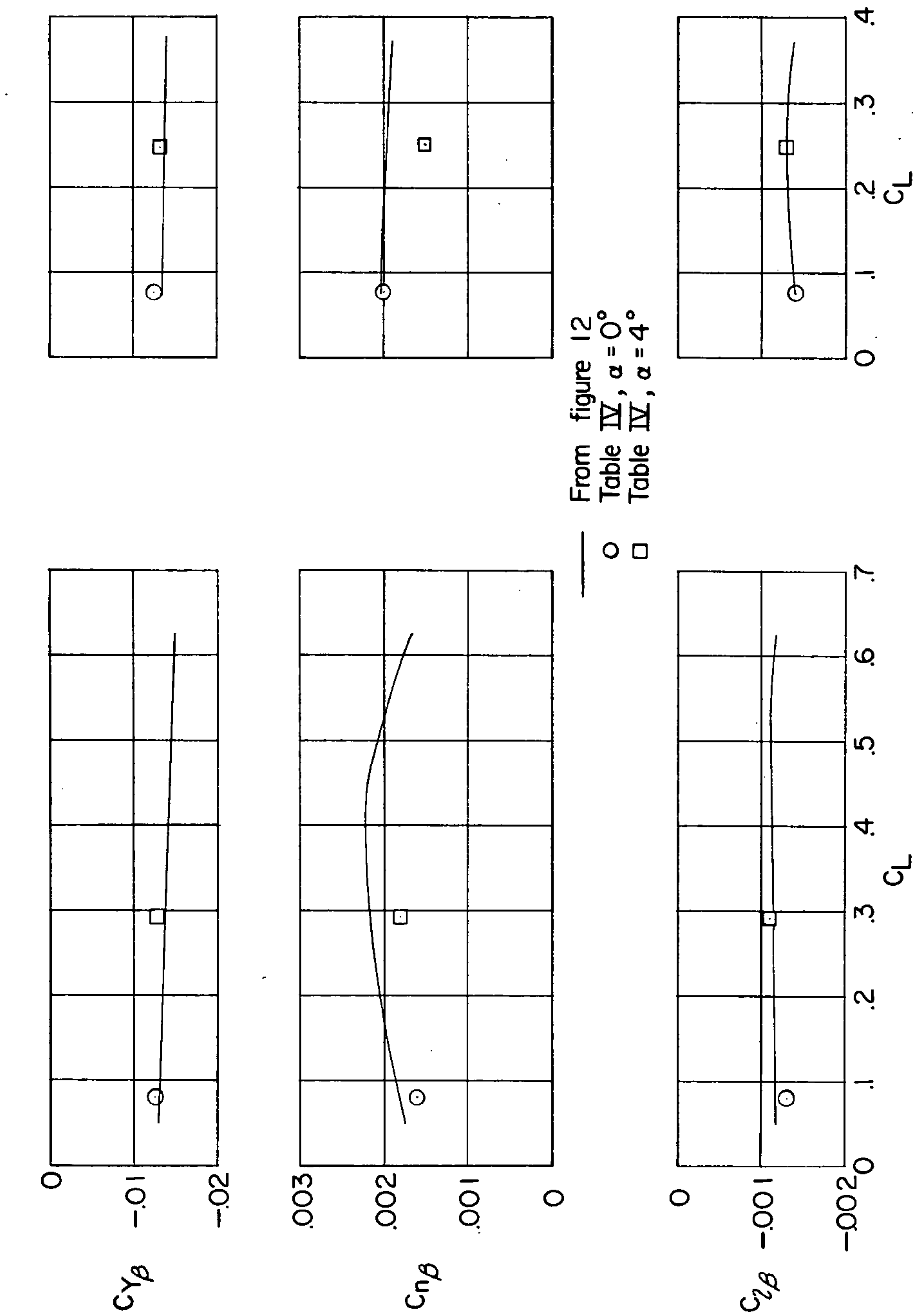

(a) M = 1.61.

(b) M = 2.01.

Figure 13.- Variation of sideslip derivatives with lift coefficient. Complete model; $\delta_r = 0^\circ$.

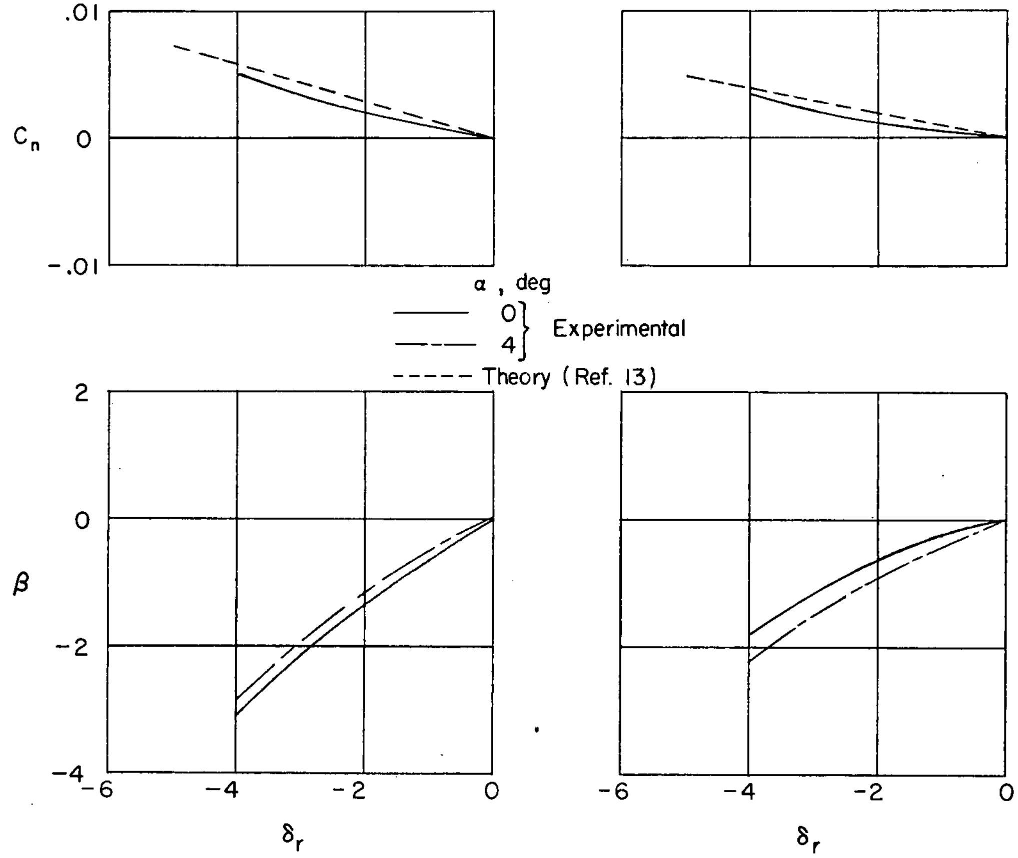

(a) M = 1.61. (b) M = 2.01.

Figure 14.- Variation of sideslip angle and yawing-moment coefficient with rudder angle. Complete model.

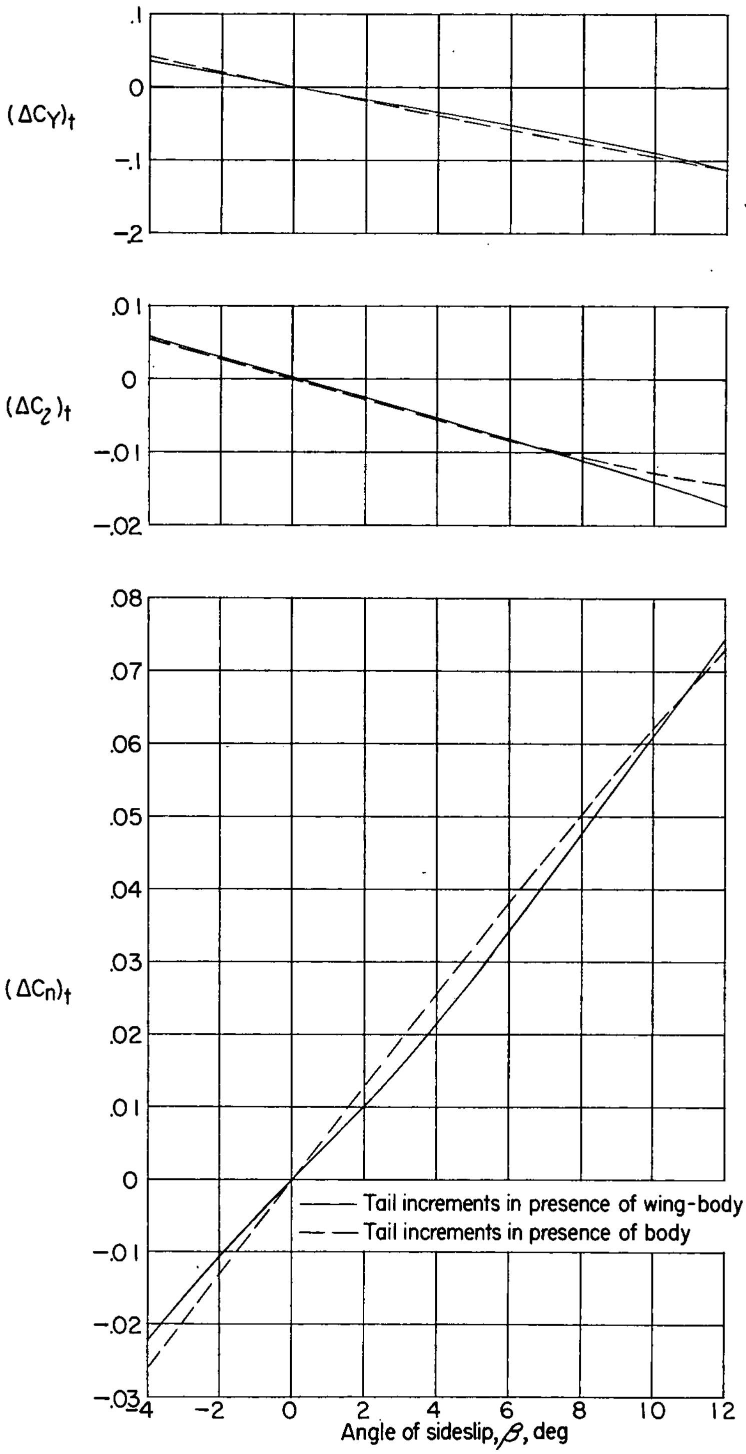

(a) M = 1.61.

Figure 15.- Effect of the wing on the incremental lateral coefficients produced by the vertical tail. $\alpha = 0^{\circ}$.

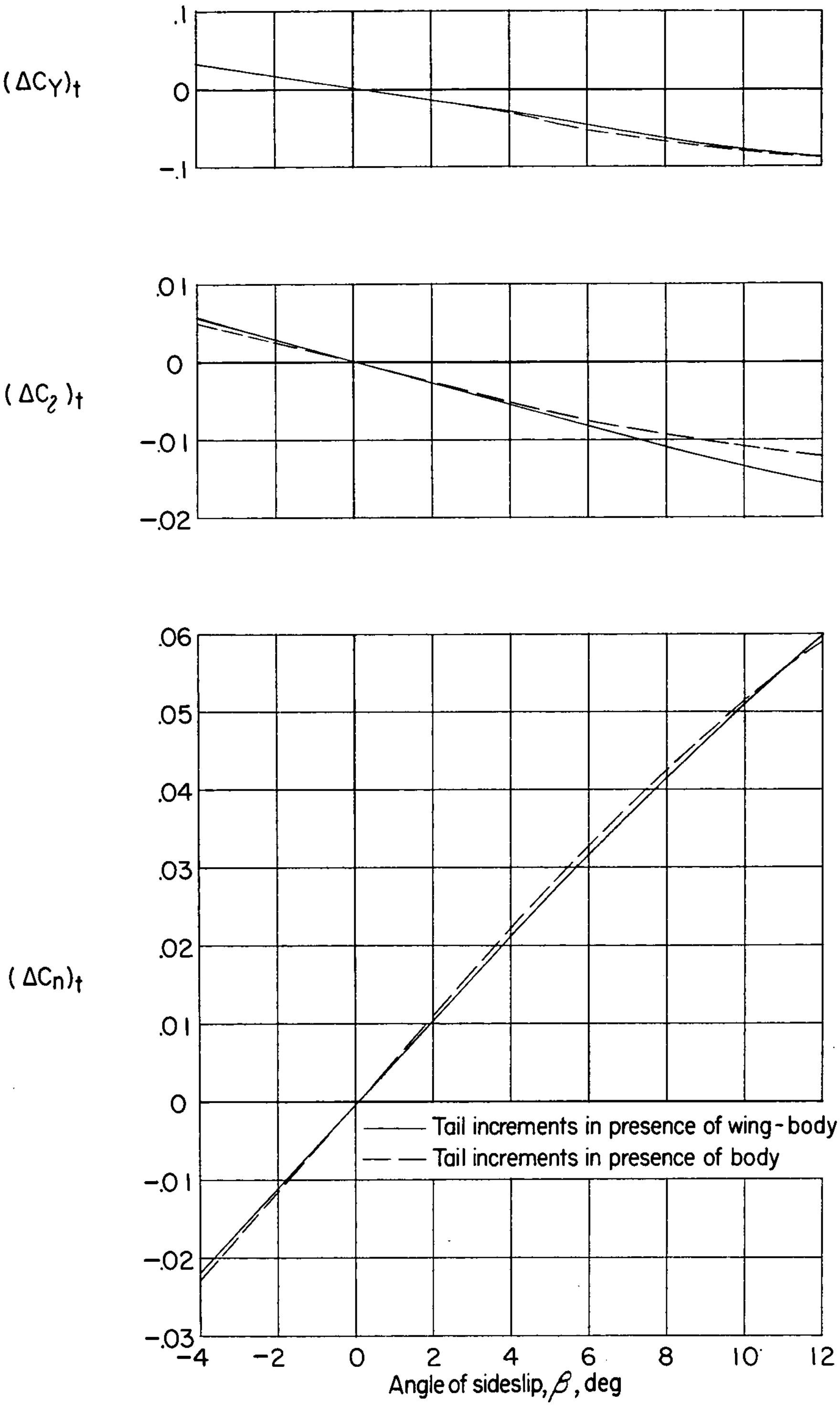

(b) M = 2.01.

Figure 15.- Concluded.

NACA-Langley - 11-4-53 - 325